

# Ternary CdS/Au/3DOM-SrTiO<sub>3</sub> composites with synergistic enhancement for hydrogen production from visible-light photocatalytic water splitting

Yue Chang <sup>a,b</sup>, Kai Yu <sup>a,c,\*</sup>, Chenxi Zhang <sup>b</sup>, Zequn Yang <sup>a</sup>, Yajun Feng <sup>a</sup>, He Hao <sup>b</sup>, Yuanzhi Jiang <sup>b</sup>, Lan-Lan Lou <sup>b</sup>, Wuzong Zhou <sup>c</sup>, Shuangxi Liu <sup>b,d,\*\*</sup>

<sup>a</sup> MOE Key Laboratory of Pollution Processes and Environmental Criteria, College of Environmental Science and Engineering, Nankai University, Tianjin 300350, People's Republic of China

<sup>b</sup> Institute of New Catalytic Materials Science and MOE Key Laboratory of Advanced Energy Materials Chemistry, School of Materials Science and Engineering, National Institute of Advanced Materials, Nankai University, Tianjin 300350, People's Republic of China

<sup>c</sup> School of Chemistry, University of St Andrews, Fife KY16 9ST, United Kingdom

<sup>d</sup> Collaborative Innovation Center of Chemical Science and Engineering (Tianjin), Tianjin 300072, People's Republic of China

## ARTICLE INFO

### Article history:

Received 14 February 2017

Received in revised form 6 May 2017

Accepted 19 May 2017

Available online 22 May 2017

### Keywords:

Three-dimensionally ordered macroporous material  
CdS/Au/3DOM-SrTiO<sub>3</sub>  
Ternary composite  
Hydrogen production from water splitting  
Slow photon effect

## ABSTRACT

New ternary composites based on three dimensionally ordered macroporous (3DOM) SrTiO<sub>3</sub> (CdS/Au/3DOM-SrTiO<sub>3</sub>) were prepared and used as photocatalysts in visible light ( $\lambda > 420$  nm) photocatalytic water splitting for hydrogen evolution. Through optimizing the pore size of 3DOM-SrTiO<sub>3</sub> materials and the loading amounts of Au and CdS, CdS/Au/3DOM-SrTiO<sub>3</sub>(300), templated by 300 nm sized poly(methyl methacrylate) colloids, was found to exhibit a remarkably enhanced photocatalytic hydrogen evolution rate (2.74 mmol/h·g), which was 3.2 times as high as that of CdS/Au/C-SrTiO<sub>3</sub> catalyst based on commercial SrTiO<sub>3</sub>. This notably enhanced photocatalytic performance was mainly attributed to the slow photon enhancement effect of 3DOM-SrTiO<sub>3</sub>(300) material, which significantly promoted the light harvesting efficiency of ternary composite for the slow photon region of 3DOM-SrTiO<sub>3</sub>(300) was well matched with the optical absorption band of photocatalyst. Further depositing Pt nanoparticles on CdS/Au/3DOM-SrTiO<sub>3</sub>(300) composite as a co-catalyst, an extraordinarily high hydrogen evolution rate (up to 5.46 mmol/g·h) and apparent quantum efficiency (42.2% at 420 nm) were achieved because of the synergistic effect of efficient carrier separation, Au SPR effect, and slow photon effect. Furthermore, these ternary CdS/Au/3DOM-SrTiO<sub>3</sub> composite photocatalysts were very stable and could be easily recycled four times in visible light photocatalytic water splitting experiments without any loss in activity.

© 2017 Elsevier B.V. All rights reserved.

## 1. Introduction

Since photocatalytic water splitting into hydrogen by TiO<sub>2</sub> was discovered by Fujishima and Honda in the early 1970s [1], hydrogen production from water splitting has become one of the most promising strategies in scientific and technological research for utilizing renewable solar energy to solve the issues of energy crisis and environmental pollution [2–5]. However, because of the low

quantum yield and light harvesting efficiency of conventional photocatalysts, especially in the visible light range, it is still a huge challenge to develop a highly efficient catalyst for photocatalytic water splitting.

Perovskite strontium titanate (SrTiO<sub>3</sub>), one of the most important n-type semiconductors, has been widely investigated owing to its efficient photocatalytic properties, structural flexibility, good stability and low cost [6–12]. However, the wide band gap of SrTiO<sub>3</sub> (ca. 3.2 eV) makes it unsuitable to be motivated by visible light, leading to a low solar energy conversion efficiency. Combination of SrTiO<sub>3</sub> with narrow band-gap semiconductors would be an effective approach to address this issue [13–15]. In this respect, cadmium sulfide (CdS) has been regarded as an ideal candidate because of its narrow band gap (2.4 eV) and more negative conduction band edge than the reduction potential of H<sup>+</sup> to H<sub>2</sub> [16–19]. Meanwhile, the obtained heterostructured photocatalysts were found to be able

\* Corresponding author at: College of Environmental Science and Engineering, Nankai University, 38 Tongyan Road, Jinnan District, Tianjin 300350, People's Republic of China.

\*\* Corresponding author at: School of Materials Science and Engineering, Nankai University, 38 Tongyan Road, Jinnan District, Tianjin 300350, People's Republic of China.

E-mail addresses: [kaiyu@nankai.edu.cn](mailto:kaiyu@nankai.edu.cn) (K. Yu), [sxliu@nankai.edu.cn](mailto:sxliu@nankai.edu.cn) (S. Liu).

to facilitate the spatial separation of photogenerated electron-hole pairs, further improving their charge utilization efficiency [20–22].

On the other hand, depositing noble metal, such as Au, in between two semiconductors to form a ternary composite, could further increase their photocatalytic performance due to the facilitated transfer of photogenerated carriers [23,24]. Moreover, the surface plasmon resonance (SPR) of metal nanoparticles arising from the collective oscillation of electrons in the metallic nanostructure could also improve the performance of photocatalysts through hot electron transfer [25–31]. Many researchers had attempted to fabricate the ternary composites using two semiconductors and one noble metal, such as Au/CdS/TiO<sub>2</sub> [23,32–37], Au/CdS/WO<sub>3</sub> [38,39], Pt/CdS/TiO<sub>2</sub> [40–45], and Au/CdS/ZnO [46–48]. However, improving the light harvesting efficiency through a special nanostructure design is still an attractive research field.

In the last decade, three-dimensionally ordered macroporous (3DOM) materials with an inverse opal structure have received much attention in photocatalysis field. A series of 3DOM semiconductors including TiO<sub>2</sub> [49–51], WO<sub>3</sub> [52,53], InVO<sub>4</sub> [54–56], BiVO<sub>4</sub> [57–59], and g-C<sub>3</sub>N<sub>4</sub> [35] have been fabricated and applied in the degradation of organic pollutants and the production of hydrogen and/or oxygen from water splitting. Notably improved photocatalytic performances were achieved over these 3DOM photocatalysts because of their slow photon effect as a photonic crystal, which could significantly enhance the photon-matter interaction, and further improve the light energy conversion efficiency of semiconductor [60–63].

Recently, we reported the 3DOM-SrTiO<sub>3</sub> materials with notably improved catalytic performance for hydrogen evolution via water splitting compared with solid-state SrTiO<sub>3</sub> under UV-vis light irradiation [64]. In order to further extend their visible light absorption and develop a highly efficient visible-light-driven photocatalyst, herein, we designed and fabricated a novel form of catalysts: CdS/Au/3DOM-SrTiO<sub>3</sub> ternary composites. The influences of CdS/Au composite ratio and pore size of 3DOM-SrTiO<sub>3</sub> were investigated. An extraordinarily excellent efficiency for visible-light-driven photocatalytic hydrogen evolution can be expected over these ternary CdS/Au/3DOM-SrTiO<sub>3</sub> composites because of the synergistic effect of slow photon effect, efficient charge separation and hot electron transfer enhancement.

## 2. Experimental

### 2.1. Materials

Tetrabutyl titanate [Ti(OBu)<sub>4</sub>], cadmium nitrate tetrahydrate [Cd(NO<sub>3</sub>)<sub>2</sub>·4H<sub>2</sub>O], gold(III) chloride hydrate (HAuCl<sub>4</sub>·4H<sub>2</sub>O), and chloroplatinic acid hexahydrate (H<sub>2</sub>PtCl<sub>6</sub>·6H<sub>2</sub>O) were purchased from Aladdin. Acetic acid (CH<sub>3</sub>COOH) and methanol (CH<sub>3</sub>OH) were acquired from Concord Technology (Tianjin) Co., Ltd. Strontium nitrate [Sr(NO<sub>3</sub>)<sub>2</sub>] was purchased from Tianjin Bodi Chemical Co., Ltd. Citric acid monohydrate (C<sub>6</sub>H<sub>8</sub>O<sub>7</sub>·H<sub>2</sub>O), trisodium citrate dihydrate (Na<sub>3</sub>C<sub>6</sub>H<sub>5</sub>O<sub>7</sub>·2H<sub>2</sub>O), sodium sulfite (Na<sub>2</sub>SO<sub>3</sub>), and sodium sulfide hydrate (Na<sub>2</sub>S·9H<sub>2</sub>O) were obtained from Tianjin Guangfu Fine Chemical Research Institute. Commercial SrTiO<sub>3</sub> (C-SrTiO<sub>3</sub>) was provided by Energy Chemical. All of the reagents were of analytical grade and used as received.

### 2.2. Characterization

The X-ray powder diffraction (XRD) patterns of the photocatalysts were obtained on the Bruker D8 X-ray diffractometer with Cu K $\alpha$  radiation operating at 40 kV and 40 mA over 2 $\theta$  range of 10°–90°. The JEOL JSM-7500F field-emission scanning electron

microscope (SEM) was employed in order to observe the morphology of samples. The images of high-resolution transmission electron microscopy (HRTEM) were acquired using a Philips Tecnai G2 F30 instrument. Diffuse-reflectance UV-vis (DR UV-vis) spectra were recorded on a Shimadzu UV-2550 spectrophotometer with the integral sphere in the measurement range from 200 nm to 800 nm. Photoluminescence (PL) spectra were carried out employing an Edinburgh Instrument FLS 920P fluorescence spectrophotometer. The online gas chromatography (GC) analysis in photocatalytic hydrogen evolution experiments was performed on a FL9790II gas chromatograph equipped with a thermal conductive detector (TCD) and a carbon molecular sieve column, using argon as the carrier gas. The photocurrent-time characteristic, electrochemical impedance spectroscopy (EIS) and Mott-Schottky measurement of these photocatalysts were carried out on a CHI 660D electrochemical workstation in a standardized three-electrode-configuration. The photocatalyst on a FTO glass was used as the working electrode. And a platinum plate and an Ag/AgCl electrode were served as the counter electrode and reference electrode, respectively.

### 2.3. Synthesis of 3DOM-SrTiO<sub>3</sub>

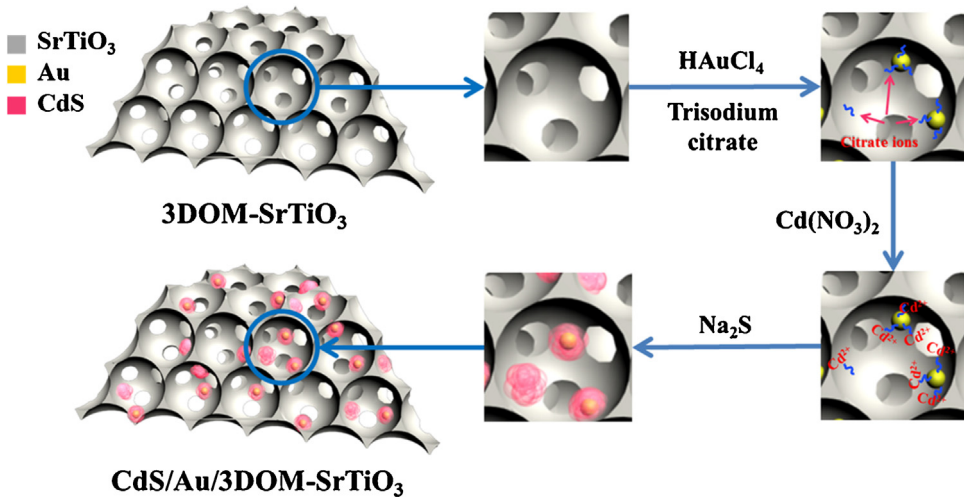
The poly methyl methacrylate (PMMA) colloidal crystal templates with average diameters of 200 nm, 300 nm, and 400 nm, and the 3DOM-SrTiO<sub>3</sub> materials with different pore sizes were synthesized according to our previous reports [53,64]. More specifically, firstly, the precursor solution was prepared as follows. 10 mL of acetic acid was added to 0.01 mol of Ti(OBu)<sub>4</sub> under stirring, followed by the dropping of 10 mL of deionized water. Then, 10 mL of Sr(NO<sub>3</sub>)<sub>2</sub> solution (1 mol/L) and 10 mL of citric acid solution (2 mol/L) were consecutively added into this mixture at room temperature and the precursor solution was obtained. Secondly, the PMMA colloidal crystal template was placed into this precursor solution. After 2 h, the impregnated colloidal crystal template was filtrated to remove the redundant precursor solution. The sample was dried in a vacuum oven at 50 °C for 12 h and then calcined in air using tube furnace at 650 °C for 4 h. According to the diameters of PMMA microspheres (200, 300, and 400 nm), the as-synthesized 3DOM-SrTiO<sub>3</sub> materials were named as 3DOM-SrTiO<sub>3</sub>(200), 3DOM-SrTiO<sub>3</sub>(300) and 3DOM-SrTiO<sub>3</sub>(400), respectively.

### 2.4. Synthesis of ternary CdS/Au/3DOM-SrTiO<sub>3</sub> composites

The synthesis procedure of ternary CdS/Au/3DOM-SrTiO<sub>3</sub> composites is shown in Scheme 1.

Au nanoparticles were decorated on the surface of 3DOM-SrTiO<sub>3</sub> through a chemical deposition method, and the typical synthesis procedure was described as follows. 0.15 g of 3DOM-SrTiO<sub>3</sub> was dispersed into 75 mL of deionized water, and a certain amount of HAuCl<sub>4</sub> solution (10 g/L) was added into this mixture at 110 °C under vigorous stirring for 0.5 h. Then, 1.5 mL of trisodium citrate aqueous solution (0.034 mol/L) was added to the flask twice every 15 min. After stirring for 1 h, the mixture was cooled down to room temperature. The purple Au/3DOM-SrTiO<sub>3</sub> solid sample was collected by centrifugation and washed with deionized water for once. The nominal Au loading amount in Au/3DOM-SrTiO<sub>3</sub> samples was 0.5%, 1.0%, 1.5%, or 2.0% in weight.

CdS/Au/3DOM-SrTiO<sub>3</sub> composites were fabricated through a deposition-precipitation method. Au/3DOM-SrTiO<sub>3</sub> was dispersed into 12 mL of Cd(NO<sub>3</sub>)<sub>2</sub>·4H<sub>2</sub>O aqueous solution under vigorous stirring for 0.5 h, and then Na<sub>2</sub>S aqueous solution was dropwise added. After stirring for 0.5 h, the obtained precipitate was collected by centrifugation, washed with deionized water for several times, and dried at 50 °C for 12 h. The obtained samples were marked as CdS/Au/3DOM-SrTiO<sub>3</sub>(200), CdS/Au/3DOM-SrTiO<sub>3</sub>(300), and



**Scheme 1.** The synthesis procedure of ternary CdS/Au/3DOM-SrTiO<sub>3</sub> composites.

CdS/Au/3DOM-SrTiO<sub>3</sub>(400). The nominal CdS loading amount in CdS/Au/3DOM-SrTiO<sub>3</sub> samples was 5%, 15%, or 20% in weight.

Because Au nanoparticles were deposited on the surface of 3DOM-SrTiO<sub>3</sub> through trisodium citrate reduction, the obtained Au nanoparticles were covered by citrate ions. Then these citrate ions could prior capture Cd<sup>2+</sup> and further lead to the coverage of CdS on the surface of Au nanoparticles. This process has been reported by Zhao et al. [35].

For comparison, commercial SrTiO<sub>3</sub> was used to prepare the ternary composite under the same synthesis procedure with CdS/Au/3DOM-SrTiO<sub>3</sub>. And the obtained photocatalyst was marked as CdS/Au/C-SrTiO<sub>3</sub>.

## 2.5. Photocatalytic hydrogen evolution experiments

The photocatalytic performance of as-prepared composite photocatalysts was determined by the hydrogen evolution experiments at room temperature under visible light irradiation. In a typical process, 0.1 g of photocatalyst and 100 mL of water containing Na<sub>2</sub>SO<sub>3</sub> (0.10 M) and Na<sub>2</sub>S (0.10 M) as the sacrificial reagents were added in a 150 mL quartz flask under stirring. After the reaction system was thoroughly degassed, the flask was irradiated by a 300 W Xe lamp (CEL-HXUV300) with a UV cut-off filter ( $\lambda > 420$  nm). The generated hydrogen was monitored by online GC.

## 3. Results and discussion

### 3.1. Characterization of as-synthesized CdS/Au/3DOM-SrTiO<sub>3</sub> composites

The as-synthesized CdS/Au/3DOM-SrTiO<sub>3</sub> photocatalysts were characterized by XRD, SEM, TEM, and DR UV-vis.

The XRD patterns of CdS/Au/3DOM-SrTiO<sub>3</sub> and CdS/Au/C-SrTiO<sub>3</sub> are shown in Fig. 1. The characteristic diffraction peaks of 3DOM-SrTiO<sub>3</sub> for three CdS/Au/3DOM-SrTiO<sub>3</sub> samples can be well indexed to the (100), (110), (111), (200), (211), (220) and (310) crystal planes of pure cubic perovskite phase (JCPDS No. 35-0734). Expect the diffraction peaks of 3DOM-SrTiO<sub>3</sub>, the weak and wide diffraction peak at about 26.5° (marked with ♦) on the patterns of CdS/Au/3DOM-SrTiO<sub>3</sub> could be resulted from overlapped diffraction peaks of the (100), (002), and (101) planes of the greenockite structured CdS, suggesting the presence of CdS. The diffraction peak of Au (111) at 38.1° is also observed from Fig. 1, corroborating the successful deposition of Au nanoparticles on the surface of 3DOM-SrTiO<sub>3</sub>. In addition, the XRD peak intensities of

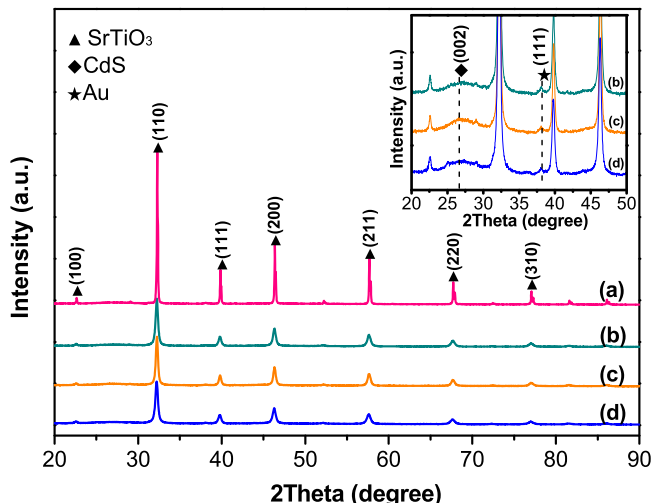


**Fig. 1.** Powder XRD patterns of (a) CdS/Au/C-SrTiO<sub>3</sub>, (b) CdS/Au/3DOM-SrTiO<sub>3</sub>(200), (c) CdS/Au/3DOM-SrTiO<sub>3</sub>(300), and (d) CdS/Au/3DOM-SrTiO<sub>3</sub>(400).

CdS/Au/3DOM-SrTiO<sub>3</sub> photocatalysts are modestly weaker than those of CdS/Au/C-SrTiO<sub>3</sub> indicating a lower crystallinity of 3DOM-SrTiO<sub>3</sub>.

The morphology of the as-synthesized 3DOM-SrTiO<sub>3</sub> and ternary CdS/Au/3DOM-SrTiO<sub>3</sub> composites were visualized through SEM, and the related images are shown in Fig. 2. Clearly, the well-ordered inverse opal structure can be observed for all the 3DOM-SrTiO<sub>3</sub> materials with different pore sizes, and the average pore diameters of 3DOM-SrTiO<sub>3</sub>(200), 3DOM-SrTiO<sub>3</sub>(300), and 3DOM-SrTiO<sub>3</sub>(400) can be determined as 120 nm, 185 nm, and 245 nm, respectively, from Fig. 2(a) to (c). After decorating CdS/Au nanoparticles, the highly ordered periodic 3DOM structures were still maintained, and the CdS/Au nanoparticles were mainly dispersed into the macropores of 3DOM-SrTiO<sub>3</sub> as seen in Fig. 2(e) to (g). Furthermore, it is found from Fig. 2(d) and (h) that the commercial SrTiO<sub>3</sub> is made up of micro-sized particles with an average size of 500 nm, and the CdS/Au nanoparticles are mainly accumulated on the surface of SrTiO<sub>3</sub> in the CdS/Au/C-SrTiO<sub>3</sub> composite. SEM-EDS elemental mapping images of these CdS/Au/3DOM-SrTiO<sub>3</sub> composites are shown in Fig. S1 of Supplementary materials.

The TEM and HRTEM images, and EDS elemental mapping of the CdS/Au/3DOM-SrTiO<sub>3</sub>(300) composite are depicted in Fig. 3. The inverse opal structure of 3DOM-SrTiO<sub>3</sub>(300) can also be clearly

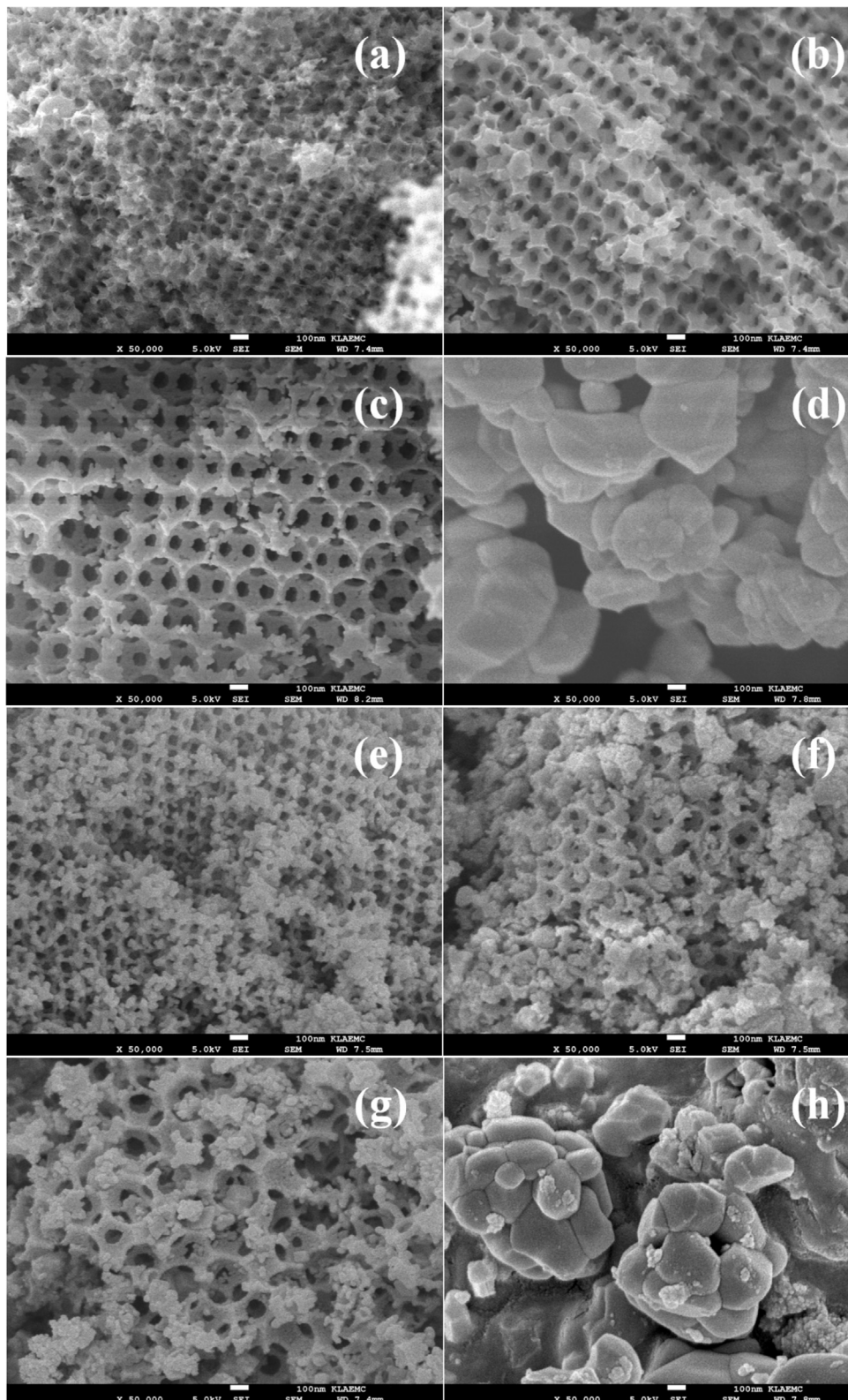


**Fig. 2.** SEM micrographs of (a) 3DOM-SrTiO<sub>3</sub>(200), (b) 3DOM-SrTiO<sub>3</sub>(300), (c) 3DOM-SrTiO<sub>3</sub>(400), (d) C-SrTiO<sub>3</sub>, (e) CdS/Au/3DOM-SrTiO<sub>3</sub>(200), (f) CdS/Au/3DOM-SrTiO<sub>3</sub>(300), (g) CdS/Au/3DOM-SrTiO<sub>3</sub>(400), and (h) CdS/Au/C-SrTiO<sub>3</sub>.

observed in the TEM image in Fig. 3(a). The average size of the Au nanoparticles is ~20 nm. Moreover, as shown in Fig. 3(b) and (c), the existence of Au and CdS in the ternary composite is directly confirmed through the measure lattice spacing corresponding to the CdS(002) and Au(111) planes. In addition, the EDS elemen-

tal mapping in a selected area indicated that Au nanoparticles were covered by CdS, which further confirmed the heterojunction structure of ternary CdS/Au/3DOM-SrTiO<sub>3</sub>(300) composite. More HRTEM images of CdS/Au/3DOM-SrTiO<sub>3</sub> composites are given in Fig. S2 of Supplementary materials.

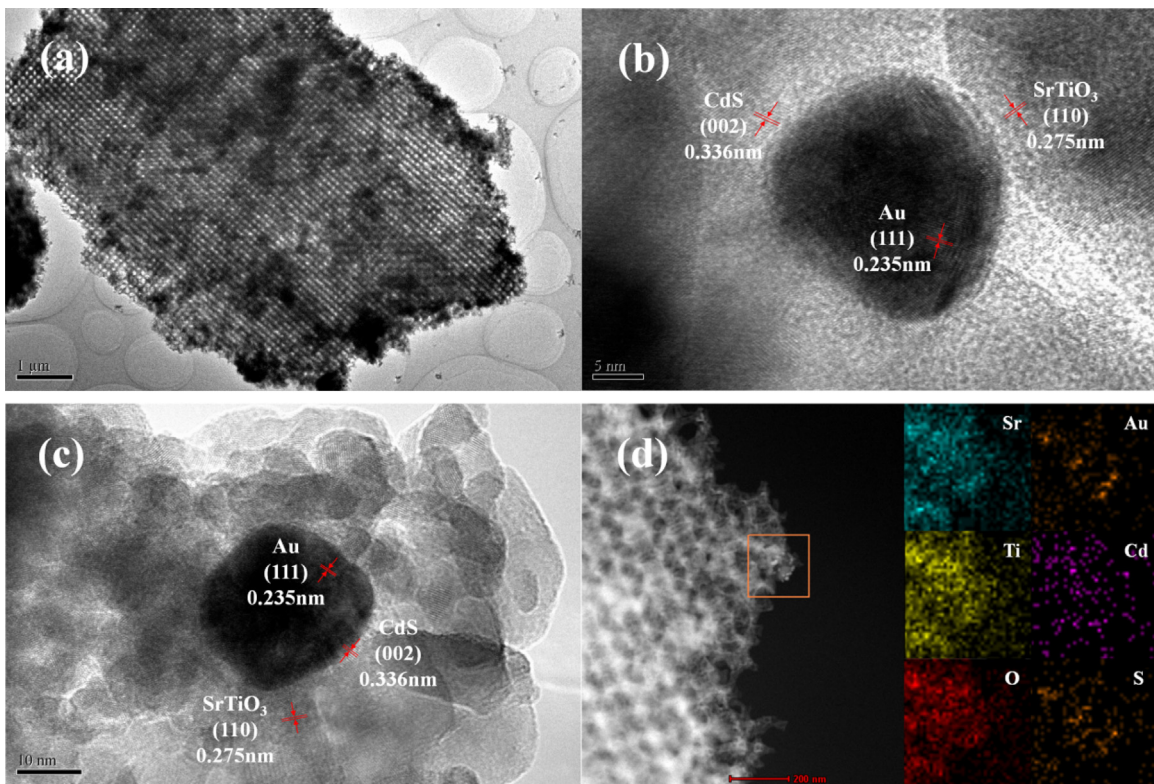


**Fig. 3.** TEM image (a), HRTEM images (b, c) and HAADF-STEM-EDS elemental mapping (d) of CdS/Au/3DOM-SrTiO<sub>3</sub>(300).

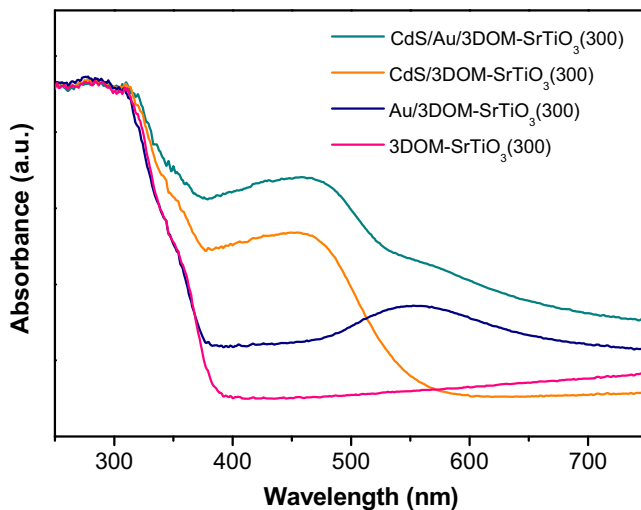


**Fig. 4.** DR UV-vis spectra of CdS/Au/3DOM-SrTiO<sub>3</sub>(300), CdS/3DOM-SrTiO<sub>3</sub>(300), Au/3DOM-SrTiO<sub>3</sub>(300) and 3DOM-SrTiO<sub>3</sub>(300).

**Fig. 4** shows the DR UV-vis spectra of 3DOM-SrTiO<sub>3</sub>(300), CdS/3DOM-SrTiO<sub>3</sub>(300), Au/3DOM-SrTiO<sub>3</sub>(300) and CdS/Au/3DOM-SrTiO<sub>3</sub>(300) samples. The optical absorption edge of 3DOM-SrTiO<sub>3</sub>(300) locates at around 380 nm. Au/3DOM-SrTiO<sub>3</sub>(300) exhibits a broad absorption peak at 550 nm, corresponding to the SPR absorption of Au nanoparticles. Because of the combination of CdS, both CdS/3DOM-SrTiO<sub>3</sub>(300) and CdS/Au/3DOM-SrTiO<sub>3</sub>(300) show a strong response in the range of 400–600 nm. It is worthy to note from **Fig. 4** that the absorption edge of the ternary CdS/Au/3DOM-SrTiO<sub>3</sub>(300) composite has an obvious redshift compared with other specimens, which can be attributed to the synergistic influence of CdS and Au.

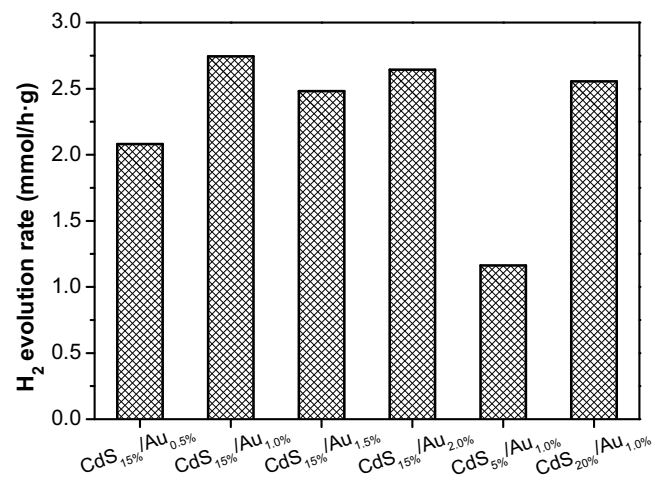


**Fig. 5.** The efficiencies of hydrogen evolution over CdS/Au/3DOM-SrTiO<sub>3</sub>(300) with different Au and CdS loading amounts under visible light irradiation ( $\lambda > 420$  nm).

### 3.2. Effect of Au and CdS loading amount on the efficiency of photocatalytic hydrogen evolution

In order to optimize the constituent of the ternary CdS/Au/3DOM-SrTiO<sub>3</sub> composites, the influence of Au and CdS loading amount on the photocatalytic efficiency of CdS/Au/3DOM-SrTiO<sub>3</sub> has been investigated. A series of CdS/Au/3DOM-SrTiO<sub>3</sub>(300) composites with different mass percentages of Au (0.5%, 1.0%, 1.5%, and 2.0%) and CdS (5%, 15% and 20%) were synthesized and used in the visible light photocatalytic water splitting. It can be found from **Fig. 5**, the hydrogen evolution rate over CdS/Au/3DOM-SrTiO<sub>3</sub>(300) obviously increases as the Au loading amount increases from 0.5 wt% to 1.0 wt%, suggesting the more efficient transfer of photogenerated carrier with increasing

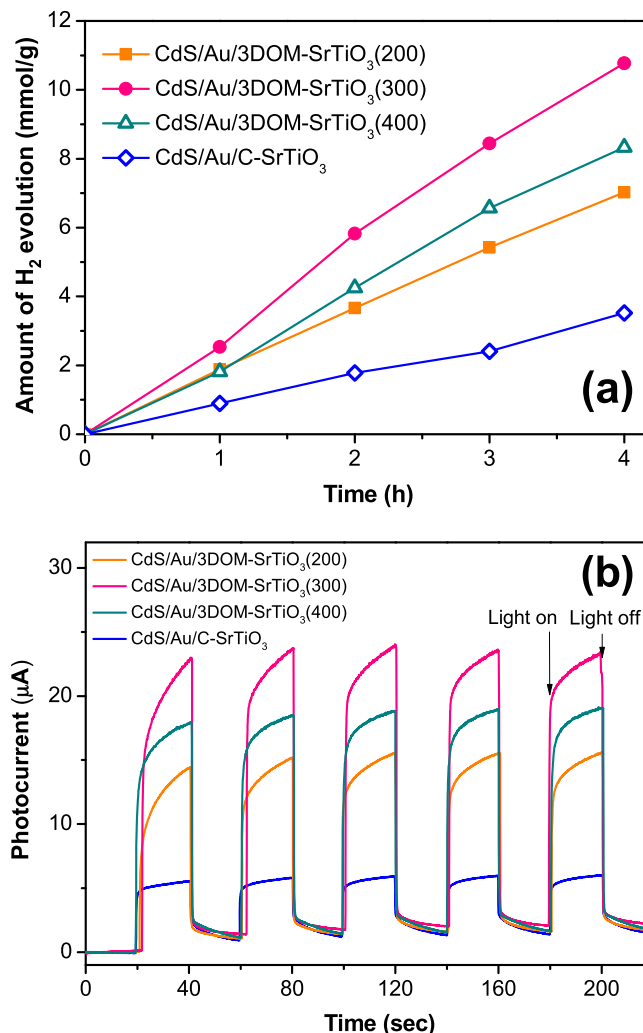


**Fig. 6.** The efficiencies of hydrogen evolution (a) and photocurrent-time (I-t) curves (b) over the CdS/Au/C-SrTiO<sub>3</sub> and CdS/Au/3DOM-SrTiO<sub>3</sub> composites with different pore sizes.

the Au loading amount. However, with further increase of the Au loading amount from 1.0 wt% to 2.0 wt%, the hydrogen evolution rate of CdS/Au/3DOM-SrTiO<sub>3</sub>(300) catalyst slightly decreases, which could be attributed to the increased particle size of Au nanoparticles. In addition, as shown in Fig. 5, the highest hydrogen evolution rate could be obtained when the loading amount of CdS is 15 wt% in CdS/Au/3DOM-SrTiO<sub>3</sub>(300). Consequently, in this work, the optimized loading amounts of CdS and Au are found to be 15 wt% and 1.0 wt%, respectively.

### 3.3. The slow photon effect on the efficiency of photocatalytic hydrogen evolution

To study the influence of inverse opal structure on the photocatalytic activity of ternary CdS/Au/3DOM-SrTiO<sub>3</sub> composites, the specimens with different pore sizes and CdS/Au/C-SrTiO<sub>3</sub> were evaluated in the visible light photocatalytic water splitting for hydrogen evolution and the results are shown in Fig. 6(a). It can be clearly observed that all the CdS/Au/3DOM-SrTiO<sub>3</sub> catalysts exhibit notably higher photocatalytic hydrogen evolution rates than CdS/Au/C-SrTiO<sub>3</sub>. It indicates that the inverse opal structure of 3DOM-SrTiO<sub>3</sub> can remarkably enhance the photocatalytic activity of these ternary composites, which can be mainly attributed

to the following reasons. Firstly, the three dimensionally interconnected pore channels can facilitate the diffusion and mass transfer of aqueous solution containing S<sup>2-</sup> and SO<sub>3</sub><sup>2-</sup>, which can eliminate the photogenerated holes. Secondly, the skeletal wall thickness of 3DOM-SrTiO<sub>3</sub> is nano-sized, which can shorten the diffusion length of photogenerated carriers so as to prevent carriers' recombination. Finally, and most importantly, the 3DOM-SrTiO<sub>3</sub> materials possess an amazing slow photon effect, which increases the interaction between photons and the catalyst, leading to the enhancement of light-energy conversion efficiency.

As described in Fig. 6(a), among these ternary CdS/Au/3DOM-SrTiO<sub>3</sub> composites, CdS/Au/3DOM-SrTiO<sub>3</sub>(300) exhibits the highest hydrogen evolution rate, up to 2.74 mmol/g·h, which is 3.2 times as high as that of CdS/Au/C-SrTiO<sub>3</sub> catalyst. Meanwhile, the hydrogen evolution rates of CdS/Au/3DOM-SrTiO<sub>3</sub>(200) and CdS/Au/3DOM-SrTiO<sub>3</sub>(400) are 1.76 mmol/g·h and 2.14 mmol/g·h, respectively.

A photocurrent generation measurement for CdS/Au/3DOM-SrTiO<sub>3</sub> and CdS/Au/C-SrTiO<sub>3</sub> catalysts was performed under visible light irradiation, and the results are shown in Fig. 6(b). All the samples show strong sensitivity to visible light irradiation and there is a dramatic rise for the photocurrent from the off illumination to the on illumination. In addition, the photocurrent response of CdS/Au/3DOM-SrTiO<sub>3</sub> is remarkably higher than that of CdS/Au/C-SrTiO<sub>3</sub>, which indicates the notably enhanced separation efficiency of photogenerated carriers over the CdS/Au/3DOM-SrTiO<sub>3</sub> composites. Among these ternary CdS/Au/3DOM-SrTiO<sub>3</sub> composites, CdS/Au/3DOM-SrTiO<sub>3</sub>(300) exhibits the highest photocurrent response, which is well consistent with the results of photocatalytic hydrogen evolution experiments.

In order to concretely analyze the influence of slow photon effect in the CdS/Au/3DOM-SrTiO<sub>3</sub> catalysts, the stop-bands of 3DOM-SrTiO<sub>3</sub> materials were calculated using the modified Bragg's law as described in Eq. (1) [57,64,65]. In this Eq., (1) is the wavelength of the photonic stop-band, D is the pore size derived from the inverse opals, n<sub>SrTiO<sub>3</sub></sub> and n<sub>water</sub> are the refractive index of SrTiO<sub>3</sub> and water, respectively, f is the SrTiO<sub>3</sub> phase volume percentage, which is generally given as 0.26, θ is the incident angle of light, which is in the range of 0–90° due to a varied and wide range of the incident angle under light irradiation for the photocatalysts in the reaction solution. Therefore the calculated stop-band of 3DOM-SrTiO<sub>3</sub>(300) (D = 185 nm) is in the range of 407–507 nm, while for 3DOM-SrTiO<sub>3</sub>(200) (D = 120 nm) and 3DOM-SrTiO<sub>3</sub>(400) (D = 245 nm), the stop-band ranges are about 264–329 nm and 533–663 nm, respectively.

$$\lambda = 2 \sqrt{\frac{2}{3} D \sqrt{n_{SrTiO_3}^2 f + n_{water}^2 (1-f) - \sin^2 \theta}} \quad (1)$$

According to the related literatures [34,66,67], the group velocity of light could dramatically reduce at the edges of stop-band and result in the appearance of slow photons. Especially, the red-edge of stop-band for inverse opals is thought to be more important in photocatalysis because of the relative higher refractive index of skeletal material. In the present work, because of the varied incident angle in the range of 0–90°, the stop-bands of these 3DOM-SrTiO<sub>3</sub> materials were variable in a wide range [68,69]. It would result in a wide slow photon region at the red-edges of stop-band, and this slow photon region was partially overlapped with its stop-band. Fig. 7(a) depicts the UV-vis spectra of these CdS/Au/3DOM-SrTiO<sub>3</sub> composites. It can be found that the CdS/Au/3DOM-SrTiO<sub>3</sub> composites exhibit a strong absorption at the wavelength from 400 to 500 nm, which was exactly overlapped with the slow photon region of 3DOM-SrTiO<sub>3</sub>(300) material. However, the slow photon region of 3DOM-SrTiO<sub>3</sub>(200) is in the range of ultraviolet light and the

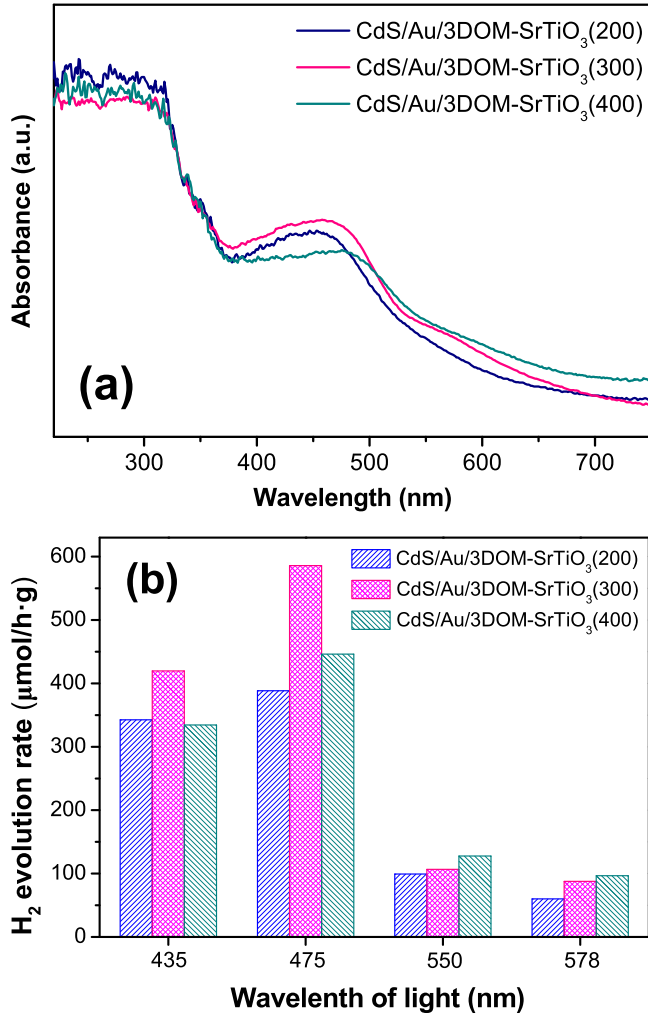


**Fig. 7.** (a) DR UV-vis spectra of CdS/Au/3DOM-SrTiO<sub>3</sub> composites. (b) The efficiencies of hydrogen evolution over CdS/Au/3DOM-SrTiO<sub>3</sub> under the certain wavelength light irradiation.

slow photon region of 3DOM-SrTiO<sub>3</sub>(400) oversteps the absorption region of these CdS/Au/3DOM-SrTiO<sub>3</sub> composites.

In order to further prove the influence of slow photon effect on the hydrogen evolution efficiency upon CdS/Au/3DOM-SrTiO<sub>3</sub> catalysts, the controlled experiments over these composites were carried out under the certain wavelength light irradiation, including 435 nm, 475 nm, 550 nm, and 578 nm. It can be found from Fig. 7(b) that CdS/Au/3DOM-SrTiO<sub>3</sub>(300) exhibits the highest photocatalytic hydrogen evolution rate under irradiation of 435 nm and 475 nm light. The result can be attributed to the proper slow photon region of 3DOM-SrTiO<sub>3</sub>(300), which could significantly increase the photon-matter interaction and further improve the photocatalytic performance of CdS/Au/3DOM-SrTiO<sub>3</sub>(300). When the water splitting experiments were carried out under the irradiation of 550 nm or 578 nm light, CdS/Au/3DOM-SrTiO<sub>3</sub>(400) exhibits slightly higher hydrogen evolution rates compared with the other two catalysts because of the overlap between incident light wavelength and slow photon region of 3DOM-SrTiO<sub>3</sub>(400). It is a direct experimental evidence for the slow light enhancement effect on these ternary CdS/Au/3DOM-SrTiO<sub>3</sub> composites and also directly proves the conclusion that the overlap of slow photon region with the electronic absorption band would significantly improve the photocatalytic performance of CdS/Au/3DOM-SrTiO<sub>3</sub> composites.

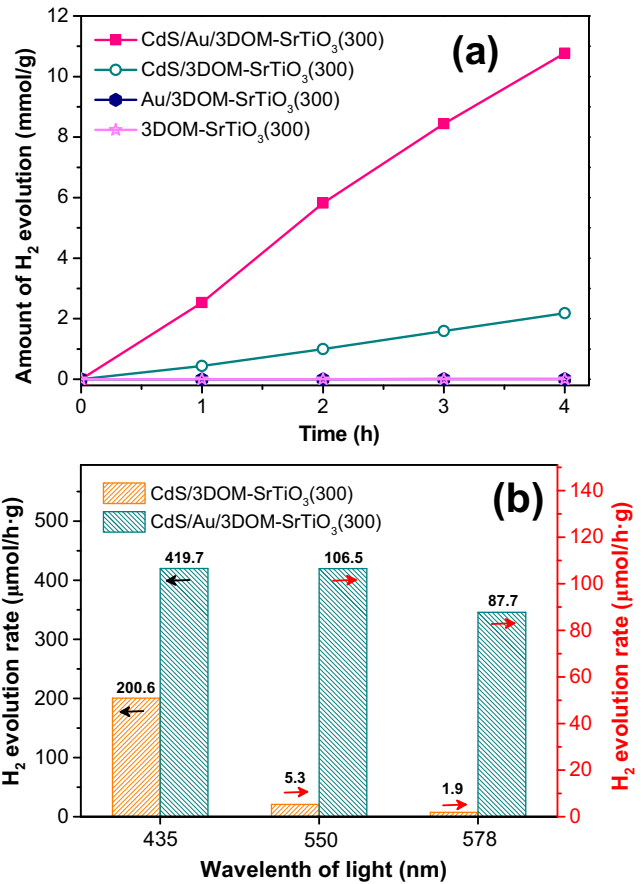


**Fig. 8.** The efficiencies of hydrogen evolution over (a) unary, binary, and ternary photocatalysts based on 3DOM-SrTiO<sub>3</sub>(300) and (b) CdS/3DOM-SrTiO<sub>3</sub>(300) and CdS/Au/3DOM-SrTiO<sub>3</sub>(300) under the certain wavelength light irradiation.

### 3.4. The roles of Au nanoparticles in ternary CdS/Au/3DOM-SrTiO<sub>3</sub> composites

Besides the slow photon effect of 3DOM-SrTiO<sub>3</sub> materials, the efficient separation of photogenerated carriers and the SPR effect of Au nanoparticles in these ternary CdS/Au/3DOM-SrTiO<sub>3</sub> photocatalysts are also important factors in enhancing the photocatalytic performance. In order to comprehend the roles of Au in ternary composites, 3DOM-SrTiO<sub>3</sub>(300) and binary composites, including Au/3DOM-SrTiO<sub>3</sub>(300) and CdS/3DOM-SrTiO<sub>3</sub>(300), were used as photocatalysts in water splitting experiments. In this experiment, CdS/3DOM-SrTiO<sub>3</sub>(300) was prepared through a deposition-precipitation method similar with that of CdS/Au/3DOM-SrTiO<sub>3</sub>(300), except that Au/3DOM-SrTiO<sub>3</sub>(300) was replaced by 3DOM-SrTiO<sub>3</sub>(300).

It is evident from Fig. 8(a) that 3DOM-SrTiO<sub>3</sub>(300) is inactive in this visible-light-driven photocatalytic water splitting experiment due to its wide band gap. While Au/3DOM-SrTiO<sub>3</sub>(300) exhibits a very slight activity (1.86 mmol/g·h), which could be assigned to the SPR effect of Au nanoparticles [23,30,70]. As for CdS/3DOM-SrTiO<sub>3</sub>(300), a considerable hydrogen evolution rate (0.44 mmol/g·h) is obtained under visible light irradiation because of the heterojunction structure between CdS and 3DOM-SrTiO<sub>3</sub>(300) that extended the light absorption of 3DOM-SrTiO<sub>3</sub>(300) and promoted the carrier separation efficiency. Compared with the three former photocatalysts, ternary CdS/Au/3DOM-SrTiO<sub>3</sub>(300) composite furnished the highest pho-

tocatalytic hydrogen evolution rate (2.74 mmol/g·h). This excellent performance of CdS/Au/3DOM-SrTiO<sub>3</sub>(300) could be attributed to the synergistic effect of two factors. On the one hand, the SPR effect of Au nanoparticles could improve the performance of CdS/Au/3DOM-SrTiO<sub>3</sub> through hot electron transfer [25–30]. On the other hand, the presence of Au nanoparticles between CdS and 3DOM-SrTiO<sub>3</sub> could obviously facilitate the transfer and separation of photogenerated carriers.

In order to verify these two roles of Au nanoparticles in ternary CdS/Au/3DOM-SrTiO<sub>3</sub> composites, a series of controlled experiments and characterizations were carried out in present work. Firstly, the SPR effect of Au nanoparticles can be observed from the DR UV-vis characterization of obtained photocatalysts (as shown in Fig. 4). The obvious absorption peaks centered at 550 nm in the DR UV-vis spectra of Au/3DOM-SrTiO<sub>3</sub>(300) and CdS/Au/3DOM-SrTiO<sub>3</sub>(300) can be associated with the SPR effect of Au nanoparticles. Taking into account of the absorption edge of binary CdS/3DOM-SrTiO<sub>3</sub>(300) composite located at 550 nm, a series of controlled water splitting experiments over binary CdS/3DOM-SrTiO<sub>3</sub>(300) and ternary CdS/Au/3DOM-SrTiO<sub>3</sub>(300) composites under the certain wavelength (including 435, 550, and 578 nm) light irradiation were carried out to investigate the SPR effect of Au nanoparticles. It can be found from Fig. 8(b), the hydrogen evolution rate of CdS/Au/3DOM-SrTiO<sub>3</sub>(300) was 2 times as high as that of CdS/3DOM-SrTiO<sub>3</sub>(300) when the radiation wavelength was 435 nm. However, when the radiation wavelength was 550 nm, the hydrogen evolution rate of CdS/Au/3DOM-SrTiO<sub>3</sub>(300) was 20 times higher than that of CdS/3DOM-SrTiO<sub>3</sub>(300). Further increasing the radiation wavelength to 578 nm, the hydrogen evolution efficiency ratio of CdS/Au/3DOM-SrTiO<sub>3</sub>(300) to CdS/3DOM-SrTiO<sub>3</sub>(300) reached up to 46 times. The notably enhanced photocatalytic performance of CdS/Au/3DOM-SrTiO<sub>3</sub>(300) under the light irradiation with wavelength of 550 and 578 nm can be derived from the contribution of Au SPR effect in ternary CdS/Au/3DOM-SrTiO<sub>3</sub> composites.

Secondly, the facilitated charge transfer and separation derived from Au nanoparticles can be confirmed through the PL and EIS measurements of 3DOM-SrTiO<sub>3</sub>(300), CdS/3DOM-SrTiO<sub>3</sub>(300), and CdS/Au/3DOM-SrTiO<sub>3</sub>(300) materials. Fig. 9(a) depicts the PL spectra of these samples. It can be seen that 3DOM-SrTiO<sub>3</sub>(300) exhibited the highest intensity in the PL emission spectrum. After loading CdS, the intensity of PL emission spectrum arising from the recombination of free carriers obviously decreased, which indicated that the separation efficiency of electron-hole pairs was enhanced over the binary CdS/3DOM-SrTiO<sub>3</sub>(300) composite. When Au nanoparticles were introduced between CdS and 3DOM-SrTiO<sub>3</sub>(300) to form the ternary CdS/Au/3DOM-SrTiO<sub>3</sub>(300) composite, the PL emission intensity decreased to the lowest level compared with 3DOM-SrTiO<sub>3</sub>(300) and CdS/3DOM-SrTiO<sub>3</sub>(300), implying the notably improved separation efficiency of photogenerated electron-hole pairs in ternary composite.

To further verify the efficient charge transfer in ternary composite, the EIS characterization of 3DOM-SrTiO<sub>3</sub>(300), CdS/3DOM-SrTiO<sub>3</sub>(300), and CdS/Au/3DOM-SrTiO<sub>3</sub>(300) were carried out and the results are shown in Fig. 9(b). The EIS Nyquist plot of CdS/Au/3DOM-SrTiO<sub>3</sub>(300) exhibited the smallest diameter of semicircle compared with 3DOM-SrTiO<sub>3</sub>(300) and CdS/3DOM-SrTiO<sub>3</sub>(300), suggesting that CdS/Au/3DOM-SrTiO<sub>3</sub>(300) provided more efficient charge transfer across the interface of the electrode and the electrolyte. The results of PL and EIS characterization indicated that the presence of Au nanoparticles in ternary CdS/Au/3DOM-SrTiO<sub>3</sub>(300) composite can significantly improve the transfer and separation of photogenerated carriers.

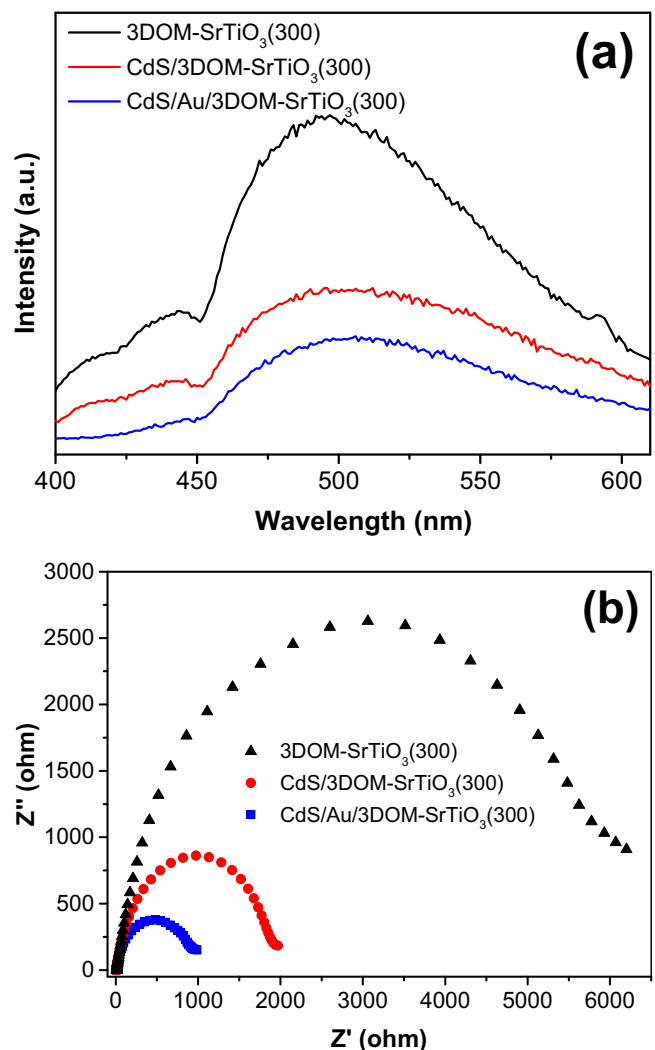
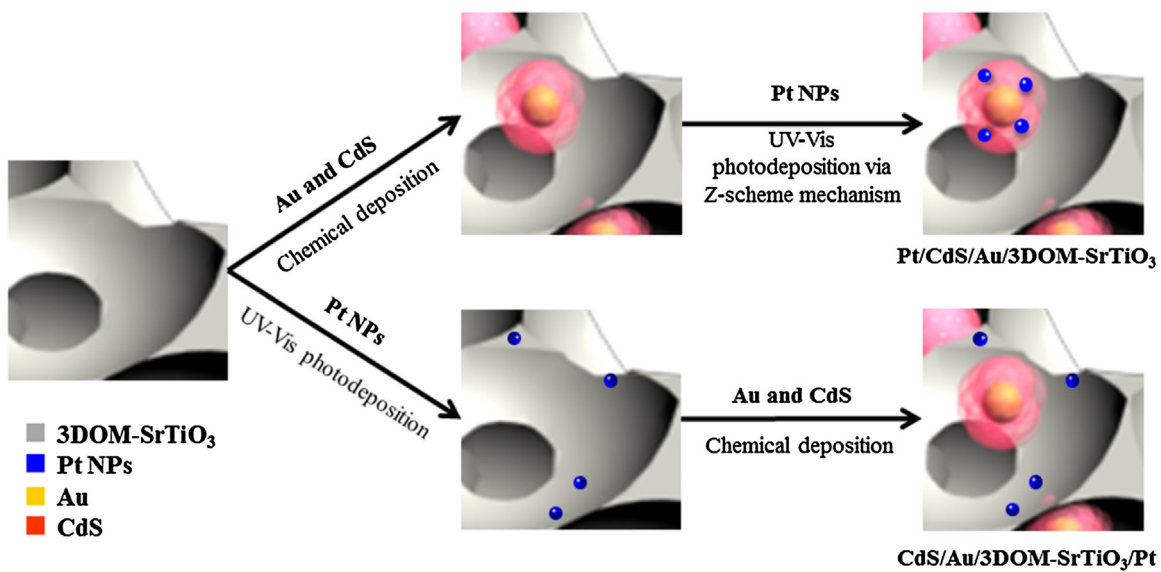


**Fig. 9.** (a) PL spectra and (b) EIS Nyquist plots of 3DOM-SrTiO<sub>3</sub>(300), CdS/3DOM-SrTiO<sub>3</sub>(300), and CdS/Au/3DOM-SrTiO<sub>3</sub>(300).

### 3.5. The photogenerated carriers transfer mechanism of ternary CdS/Au/3DOM-SrTiO<sub>3</sub> photocatalysts

In order to investigate the transfer process of photogenerated carriers for ternary CdS/Au/3DOM-SrTiO<sub>3</sub>(300) composite under visible light irradiation, two Pt nanoparticles decorated CdS/Au/3DOM-SrTiO<sub>3</sub>(300) samples were prepared according to the reported method [31]. It should be noted that the loading position of Pt nanoparticle in these two samples was different. Scheme 2 depicts the synthesis procedure of these Pt deposited CdS/Au/3DOM-SrTiO<sub>3</sub>(300) photocatalysts. For the first sample, marked as CdS/Au/3DOM-SrTiO<sub>3</sub>(300)/Pt, Pt nanoparticles (0.7 wt%) were photodeposited on the surface of 3DOM-SrTiO<sub>3</sub>(300) using methanol as the sacrificial agent under UV light irradiation before the combination of Au and CdS. For the second sample, named as Pt/CdS/Au/3DOM-SrTiO<sub>3</sub>(300), Pt nanoparticles (0.7 wt%) were in situ photodeposited on the surface of CdS via a UV-vis light driven Z-scheme process over CdS/Au/3DOM-SrTiO<sub>3</sub>(300) photocatalyst [33,34,38]. As seen in Fig. 10, the decoration of Pt nanoparticles can significantly increase the hydrogen evolution rate of the CdS/Au/3DOM-SrTiO<sub>3</sub>(300) composite. Especially by using the CdS/Au/3DOM-SrTiO<sub>3</sub>(300)/Pt catalysts, an extraordinarily high hydrogen evolution rate was achieved (up to 5.46 mmol/g·h) in visible light photocatalytic



**Scheme 2.** The synthesis procedure of Pt deposited CdS/Au/3DOM-SrTiO<sub>3</sub>(300) photocatalysts.

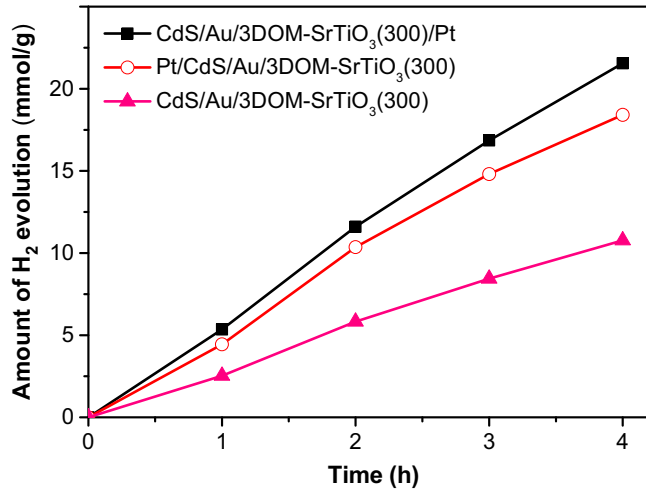


**Fig. 10.** The efficiencies of hydrogen evolution over Pt decorated CdS/Au/3DOM-SrTiO<sub>3</sub>(300) composites and the Pt free composite as a reference.

water splitting. The apparent quantum efficiency (AQE) value of CdS/Au/3DOM-SrTiO<sub>3</sub>(300)/Pt composite for hydrogen evolution was calculated by the following Eq. (2) under 420 nm wavelength light irradiation, and the calculated AQE<sub>420nm</sub> value was 42.2%. Compared with the ever reported similar catalysts based on SrTiO<sub>3</sub> [31,71–80], this is a remarkably enhanced hydrogen evolution efficiency under the similar visible-light-driven water splitting conditions (the detailed comparison was described in Supplementary materials).

$$\text{AQE} = \frac{\text{Number of reacted electrons}}{\text{Number of incident photons}} \times 100\% \quad (2)$$

In addition, CdS/Au/3DOM-SrTiO<sub>3</sub>(300)/Pt exhibited higher hydrogen evolution rate compared with Pt/CdS/Au/3DOM-SrTiO<sub>3</sub>(300) (5.46 vs. 4.72 mmol/g·h). It has been well known that Pt nanoparticles, as a co-catalyst, can provide trapping sites for the photogenerated electrons. The higher activity of CdS/Au/3DOM-SrTiO<sub>3</sub>(300)/Pt implies that the photogenerated electrons might move from CdS to 3DOM-SrTiO<sub>3</sub>(300) by a cascade of energy states. In other words, more active sites for reducing H<sup>+</sup> to H<sub>2</sub> are

generated on the surface of 3DOM-SrTiO<sub>3</sub>(300) instead of CdS. Therefore, it is logical to deduce that a favorable electron transfer pathway is CdS → Au → 3DOM-SrTiO<sub>3</sub>(300).

According to the above results, a graphic mechanism for the photocatalytic hydrogen generation process over the ternary CdS/Au/3DOM-SrTiO<sub>3</sub> composites under visible light irradiation is illustrated in Fig. 11. The redox potential of conduction bands (CB) and valence bands (VB) of as-synthesized 3DOM-SrTiO<sub>3</sub>(300) and CdS semiconductor materials were detected through Mott-Schottky measurement as described in Fig. S3 of Supplementary materials. When the CdS/Au/3DOM-SrTiO<sub>3</sub> composites were irradiated under visible light, the electrons and holes were generated on the CB and VB of CdS, respectively. Because of the more negative CB redox potential of CdS, the photogenerated electrons could transfer from the CB of CdS to that of 3DOM-SrTiO<sub>3</sub> through the conducting of Au nanoparticles. At the same time, the plasmon-induced electrons in Au nanoparticles were generated under the visible light irradiation. The plasmon-induced hot electrons migrate to the interface between Au and 3DOM-SrTiO<sub>3</sub>, and then also transfer to the CB of 3DOM-SrTiO<sub>3</sub>. The photogenerated electrons in the CB of 3DOM-SrTiO<sub>3</sub> reacted with H<sup>+</sup> in water to produce H<sub>2</sub>, and the photogenerated holes existed in the VB of CdS can oxidize the S<sup>2-</sup>/SO<sub>3</sub><sup>2-</sup> ions to S<sub>2</sub><sup>2-</sup>/SO<sub>4</sub><sup>2-</sup>.

### 3.6. Photocatalytic stability of the ternary CdS/Au/3DOM-SrTiO<sub>3</sub> composites

The stability of the as-synthesized ternary CdS/Au/3DOM-SrTiO<sub>3</sub> photocatalysts was evaluated in a cycling visible light water splitting experiment using CdS/Au/3DOM-SrTiO<sub>3</sub>(300) as a model catalyst and Na<sub>2</sub>S/Na<sub>2</sub>SO<sub>3</sub> as scavengers. Obviously, CdS/Au/3DOM-SrTiO<sub>3</sub>(300) exhibits good stability in visible-light-driven water splitting hydrogen evolution experiments (Fig. 12). At the fourth cycling experiment, the hydrogen evolution rate still remained more than 2.65 mmol/g·h. The used CdS/Au/3DOM-SrTiO<sub>3</sub>(300) catalyst after 4th recycle were characterized through XRD and SEM. The results are shown in Figs. S4 and S5 of Supplementary materials. It can be found that the 3DOM structure and the crystallinity of used CdS/Au/3DOM-SrTiO<sub>3</sub>(300) catalyst were well maintained after 4th recycle.

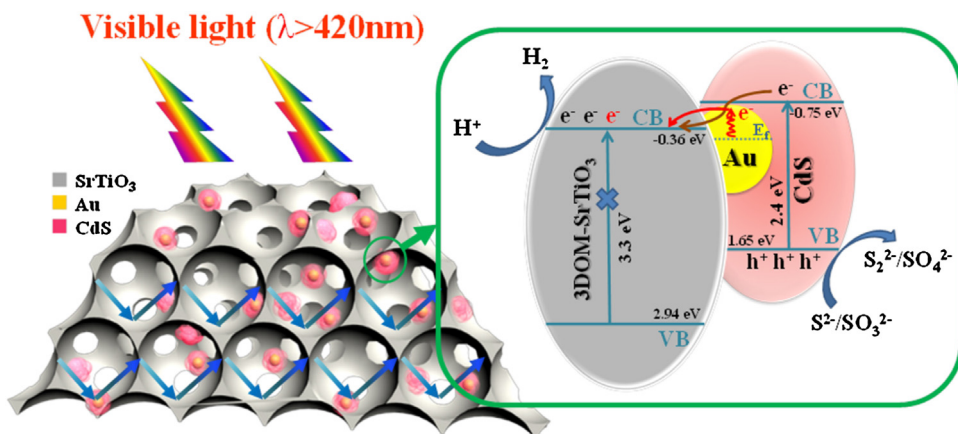


**Fig. 11.** Illustration of photogenerated carrier transfer mechanism for CdS/Au/3DOM-SrTiO<sub>3</sub> catalyst under visible light irradiation.

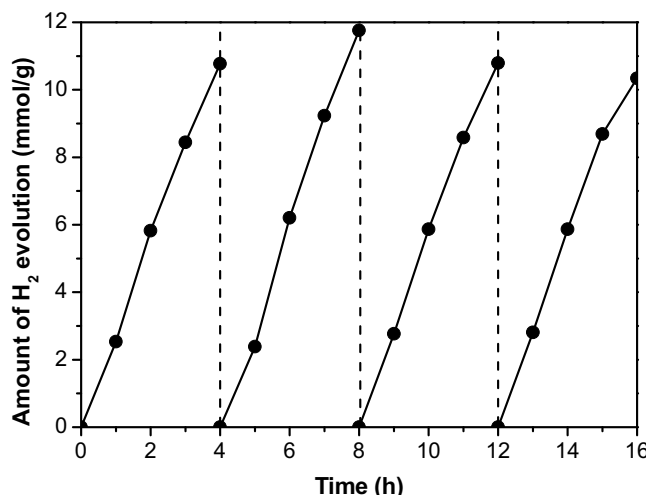


**Fig. 12.** Cycling tests of CdS/Au/3DOM-SrTiO<sub>3</sub>(300) for visible light photocatalytic hydrogen evolution from water splitting.

#### 4. Conclusions

In summary, a series of promising ternary composite photocatalysts with inverse opal structure (CdS/Au/3DOM-SrTiO<sub>3</sub>) had been successfully fabricated and well demonstrated by the characterization of XRD, SEM, TEM, DR UV-vis, and photoelectrochemical measurement. These ternary CdS/Au/3DOM-SrTiO<sub>3</sub> composites exhibited excellent performance in visible light photocatalytic water splitting for hydrogen evolution. Because of the synergistic enhancement of slow photon effect, efficient charge separation, and Au SPR effect, CdS/Au/3DOM-SrTiO<sub>3</sub>(300) exhibited a notably enhanced hydrogen evolution rate (2.74 mmol/g·h) under visible light irradiation. With further deposition of Pt nanoparticles as co-catalyst, an extraordinarily high hydrogen evolution rate of up to 5.46 mmol/g·h was achieved. Apart from these, the charge transfer mechanism in the ternary CdS/Au/3DOM-SrTiO<sub>3</sub> composites had been proposed in the present work. Moreover, these CdS/Au/3DOM-SrTiO<sub>3</sub> photocatalysts were found to be stable and could be recycled for four times without obvious loss in activity.

#### Acknowledgements

This work was supported by the National High Technology Research and Development Program of China (Grant No.

2012AA063008), the Tianjin Municipal Natural Science Foundation (Grant Nos. 17JCYBJC22600 and 15JCTPJ63500), China Scholarship Council (Grant 201606200096), and the Fundamental Research Funds for the Central Universities.

#### Appendix A. Supplementary data

Supplementary data associated with this article can be found, in the online version, at <http://dx.doi.org/10.1016/j.apcatb.2017.05.054>.

#### References

- [1] A. Fujishima, K. Honda, *Nature* 238 (1972) 37–38.
- [2] A. Kudo, Y. Miseki, *Chem. Soc. Rev.* 38 (2009) 253–278.
- [3] Z. Zou, J. Ye, K. Sayama, H. Arakawa, *Nature* 414 (2001) 625–627.
- [4] Y.Q. Qu, X.F. Duan, *Chem. Soc. Rev.* 42 (2013) 2568–2580.
- [5] K. Maeda, K. Teramura, D. Lu, T. Takata, N. Saito, Y. Inoue, K. Domen, *Nature* 440 (2006) 295.
- [6] E. Grabowska, *Appl. Catal. B* 186 (2016) 97–126.
- [7] Y. Sakata, Y. Miyoshi, T. Maeda, K. Ishikiriyama, Y. Yamazaki, H. Immura, Y. Ham, T. Hisatomi, J. Kubota, A. Yamakata, K. Domen, *Appl. Catal. A* 521 (2016) 227–232.
- [8] U. Sulaeman, S. Yin, T. Sato, *Appl. Catal. B* 105 (2011) 206–210.
- [9] R. Niishiro, S. Tanaka, A. Kudo, *Appl. Catal. B* 150–151 (2014) 187–196.
- [10] B. Wang, S. Shen, L. Guo, *Appl. Catal. B* 166–167 (2015) 320–326.
- [11] G. Zhang, G. Liu, L. Wang, J.T.S. Irvine, *Chem. Soc. Rev.* 45 (2016) 5951–5984.
- [12] W. Wang, M.O. Tade, Z. Shao, *Chem. Soc. Rev.* 44 (2015) 5371–5408.
- [13] J. Guo, S. Ouyang, P. Li, Y. Zhang, T. Kako, J. Ye, *Appl. Catal. B* 134–135 (2013) 286–292.
- [14] A.M. Schultz, P.A. Salvador, G.S. Rohrer, *Chem. Commun.* 48 (2012) 2012–2014.
- [15] D. Sharma, S. Upadhyay, V.R. Satsangi, R. Shrivastav, U.V. Waghmare, S. Dass, *J. Phys. Chem. C* 118 (2014) 25320–25329.
- [16] J.G. Yu, Y.F. Yu, P. Zhou, W. Xiao, B. Cheng, *Appl. Catal. B* 156 (2014) 184–191.
- [17] F.Q. Zhou, J.C. Fan, Q.J. Xu, Y.L. Min, *Appl. Catal. B* 201 (2017) 77–83.
- [18] T. Simon, N. Bouchonville, M.J. Berr, A. Vaneski, A. Adrovic, D. Volbers, R. Wyrwich, M. Doblinger, A.S. Susha, A.L. Rogach, F. Jackel, J.K. Stolarczyk, J. Feldmann, *Nat. Mater.* 13 (2014) 1013–1018.
- [19] N. Qin, J. Xiong, R. Liang, Y. Liu, S. Zhang, Y. Li, Z. Li, L. Wu, *Appl. Catal. B* 202 (2017) 374–380.
- [20] Y. Zhong, G. Zhao, F. Ma, Y. Wu, X. Hao, *Appl. Catal. B* 199 (2016) 466–472.
- [21] H. Zhang, X. Lv, Y. Li, Y. Wang, J. Li, *ACS Nano* 4 (2010) 380–386.
- [22] G. Wu, L. Xiao, W. Gu, W. Shi, D. Jiang, C. Liu, *RSC Adv.* 6 (2016) 19878–19886.
- [23] R. Tong, C. Liu, Z. Xu, Q. Kuang, Z. Xie, L. Zheng, *ACS Appl. Mater. Interfaces* 8 (2016) 21326–21333.
- [24] P. Zhou, J. Yu, M. Jaroniec, *Adv. Mater.* 26 (2014) 4920–4935.
- [25] S. Linic, P. Christopher, D.B. Ingram, *Nat. Mater.* 10 (2011) 911–921.
- [26] Y. Yu, Z.H. Ji, S. Zu, B.W. Du, Y.M. Kang, Z.W. Li, Z.K. Zhou, K.B. Shi, Z.Y. Fang, *Adv. Funct. Mater.* 26 (2016) 6394–6401.
- [27] Z.H. Zhang, L.B. Zhang, M.N. Hedhili, H.N. Zhang, P. Wang, *Nano Lett.* 13 (2013) 14–20.
- [28] B.H. Wu, W.T. Liu, T.Y. Chen, T.P. Perng, J.H. Huang, L.J. Chen, *Nano Energy* 27 (2016) 412–419.
- [29] Y. Shi, J. Wang, C. Wang, T.T. Zhai, W.J. Bao, J.J. Xu, X.H. Xia, H.Y. Chen, *J. Am. Chem. Soc.* 137 (2015) 7365–7370.
- [30] C.K. Song, J. Baek, T.Y. Kim, S. Yu, J.W. Han, J. Yi, *Appl. Catal. B* 198 (2016) 91–99.

- [31] S. Yu, Y.H. Kim, S.Y. Lee, H.D. Song, J. Yi, *Angew. Chem. Int. Ed.* **53** (2014) 11203–11207.
- [32] K. Song, X. Wang, Q. Xiang, J. Xu, *Phys. Chem. Chem. Phys.* **18** (2016) 29131–29138.
- [33] H. Tada, T. Mitsui, T. Kiyonaga, T. Akita, K. Tanaka, *Nat. Mater.* **5** (2006) 782–786.
- [34] Y. Wei, J. Jiao, Z. Zhao, J. Liu, J. Li, G. Jiang, Y. Wang, A. Duan, *Appl. Catal. B* **179** (2015) 422–432.
- [35] H. Zhao, M. Wu, J. Liu, Z. Deng, Y. Li, B.-L. Su, *Appl. Catal. B* **184** (2016) 182–190.
- [36] H. Zhou, L. Ding, T. Fan, J. Ding, D. Zhang, Q. Guo, *Appl. Catal. B* **147** (2014) 221–228.
- [37] H.M. Zhu, B.F. Yang, J. Xu, Z.P. Fu, M.W. Wen, T. Guo, S.Q. Fu, J. Zuo, S.Y. Zhang, *Appl. Catal. B* **90** (2009) 463–469.
- [38] X.L. Yin, J. Liu, W.J. Jiang, X. Zhang, J.S. Hu, L.J. Wan, *Chem. Commun.* **51** (2015) 13842–13845.
- [39] X. Cui, Y. Wang, G. Jiang, Z. Zhao, C. Xu, Y. Wei, A. Duan, J. Liu, J. Gao, *RSC Adv.* **4** (2014) 15689–15694.
- [40] V.M. Daskalaki, M. Antoniadou, G.L. Puma, D.I. Kondarides, P. Lianos, *Environ. Sci. Technol.* **44** (2010) 7200–7205.
- [41] J.S. Jang, S.H. Choi, H.G. Kim, J.S. Lee, *J. Phys. Chem. C* **112** (2008) 17200–17205.
- [42] M.D.O. Melo, L.A. Silva, J. Photochem. Photobiol. A **226** (2011) 36–41.
- [43] H. Park, Y.K. Kirn, W. Choi, *J. Phys. Chem. C* **115** (2011) 6141–6148.
- [44] L. Qi, J. Yu, M. Jaroniec, *Phys. Chem. Chem. Phys.* **13** (2011) 8915–8923.
- [45] Y. Wei, J. Jiao, Z. Zhao, W. Zhong, J. Li, J. Liu, G. Jiang, A. Duan, *J. Mater. Chem. A* **3** (2015) 11074–11085.
- [46] C.X. Guo, J. Xie, H. Yang, C.M. Li, *Adv. Sci.* **2** (2015) 1500135.
- [47] Z.B. Yu, Y.P. Xie, G. Liu, G.Q. Lu, X.L. Ma, H.-M. Cheng, *J. Mater. Chem. A* **1** (2013) 2773–2776.
- [48] N. Zhang, S. Xie, B. Weng, Y.-J. Xu, *J. Mater. Chem. A* **4** (2016) 18804–18814.
- [49] M. Zalfani, B. van der Schueren, M. Mahdouani, R. Bourguiga, W.B. Yu, M. Wu, O. Deparis, Y. Li, B.-L. Su, *Appl. Catal. B* **199** (2016) 187–198.
- [50] T. Wang, X. Yan, S. Zhao, B. Lin, C. Xue, G. Yang, S. Ding, B. Yang, C. Ma, G. Yang, G. Yang, *J. Mater. Chem. A* **2** (2014) 15611–15619.
- [51] M.C. Orilall, N.M. Abrams, J. Lee, F.J. DiSalvo, U. Wiesner, *J. Am. Chem. Soc.* **130** (2008) 8882–8883.
- [52] M. Sadakane, K. Sasaki, H. Kunioku, B. Ohtani, R. Abe, W. Ueda, *J. Mater. Chem.* **20** (2010) 1811–1818.
- [53] Y. Chang, K. Yu, C. Zhang, R. Li, P. Zhao, L.-L. Lou, S. Liu, *Appl. Catal. B* **176–177** (2015) 363–373.
- [54] Y. Wang, H. Dai, J. Deng, Y. Liu, H. Arandiyan, X. Li, B. Gao, S. Xie, *Solid State Sci.* **24** (2013) 62–70.
- [55] Y. Wang, H. Dai, J. Deng, Y. Liu, Z. Zhao, X. Li, H. Arandiyan, *Chem. Eng. J.* **226** (2013) 87–94.
- [56] K. Ji, J. Deng, H. Zang, J. Han, H. Arandiyan, H. Dai, *Appl. Catal. B* **165** (2015) 285–295.
- [57] K. Zhang, Y. Liu, J. Deng, S. Xie, H. Lin, X. Zhao, J. Yang, Z. Han, H. Dai, *Appl. Catal. B* **202** (2017) 569–579.
- [58] M. Zalfani, B. van der Schueren, Z.-Y. Hu, J.C. Rooke, R. Bourguiga, M. Wu, Y. Li, G. Van Tendeloo, B.-L. Su, *J. Mater. Chem. A* **3** (2015) 21244–21256.
- [59] K. Ji, J. Deng, H. Zang, J. Han, H. Arandiyan, H. Dai, *Appl. Catal. B* **165** (2015) 285–295.
- [60] X. Chen, J. Ye, S. Ouyang, T. Kako, Z. Li, Z. Zou, *ACS Nano* **5** (2011) 4310–4318.
- [61] L. Zhang, C. Baumanis, L. Robben, T. Kandiel, D. Bahnemann, *Small* **7** (2011) 2714–2720.
- [62] X. Li, X. Zhen, S. Meng, J. Xian, Y. Shao, X. Fu, D. Li, *Environ. Sci. Technol.* **47** (2013) 9911–9917.
- [63] M. Zhou, J. Bao, Y. Xu, J. Zhang, J. Xie, M. Guan, C. Wang, L. Wen, Y. Lei, Y. Xie, *ACS Nano* **8** (2014) 7088–7098.
- [64] K. Yu, C. Zhang, Y. Chang, Y. Feng, Z. Yang, T. Yang, L.-L. Lou, S. Liu, *Appl. Catal. B* **200** (2017) 514–520.
- [65] M. Wu, J. Jin, J. Liu, Z. Deng, Y. Li, O. Deparis, B.-L. Su, *J. Mater. Chem. A* **1** (2013) 15491–15500.
- [66] X. Zhang, Y. Liu, S.-T. Lee, S. Yang, Z. Kang, *Energy Environ. Sci.* **7** (2014) 1409–1419.
- [67] J. Liu, H. Zhao, M. Wu, B. Van der Schueren, Y. Li, O. Deparis, J. Ye, G.A. Ozin, T. Hasan, B.-L. Su, *Adv. Mater.* **29** (2017) 1605349.
- [68] J. Liu, J. Jin, Y. Li, H.W. Huang, C. Wang, M. Wu, L.H. Chen, B.L. Su, *J. Mater. Chem. A* **2** (2014) 5051–5059.
- [69] H. Xie, Y. Li, S. Jin, J. Han, X. Zhao, *J. Phys. Chem. C* **114** (2010) 9706–9712.
- [70] D. Lu, S.X. Ouyang, H. Xu, D.W. Li, X.L. Zhang, Y.X. Li, J.H. Ye, *ACS Appl. Mater. Interfaces* **8** (2016) 9506–9513.
- [71] H.W. Kang, S.B. Park, *Int. J. Hydrogen Energy* **41** (2016) 13970–13978.
- [72] F. Cai, Y. Meng, B. Hu, Y. Tang, W. Shi, *RSC Adv.* **5** (2015) 57354–57360.
- [73] W. Zhao, Z. Ai, X. Zhu, M. Zhang, Q. Shi, J. Dai, *Int. J. Hydrogen Energy* **39** (2014) 7705–7712.
- [74] H.W. Kang, S.B. Park, J.G. Kim, I.T. Kim, *Int. J. Hydrogen Energy* **39** (2014) 5537–5545.
- [75] P. Shen, J.C. Lofaro, W.R. Woerner, M.G. White, D. Su, A. Orlov, *Chem. Eng. J.* **223** (2013) 200–208.
- [76] Y. Jia, S. Shen, D. Wang, X. Wang, J. Shi, F. Zhang, H. Han, C. Li, *J. Mater. Chem. A* **1** (2013) 7905–7912.
- [77] S. Ouyang, H. Tong, N. Umezawa, J. Cao, P. Li, Y. Bi, Y. Zhang, J. Ye, *J. Am. Chem. Soc.* **134** (2012) 1974–1977.
- [78] H.W. Kang, S.N. Lim, D. Song, S.B. Park, *Int. J. Hydrogen Energy* **37** (2012) 11602–11610.
- [79] G. Zhang, S. Sun, W. Jiang, X. Miao, Z. Zhao, X. Zhang, D. Qu, D. Zhang, D. Li, Z. Sun, *Adv. Energy Mater.* **7** (2017) 1600932.
- [80] S. Okunaka, H. Tokudome, R. Abe, *J. Mater. Chem. A* **3** (2015) 14794–14800.